INTERNATIONAL JOURNAL OF
RADIATION ONCOLOGY • BIOLOGY • PHYSICS
www.redjournal.org

PHYSICS CONTRIBUTION

Minibeam Radiation Therapy Treatment (MBRT): Commissioning and First Clinical Implementation

Michael P. Grams, PhD,[*] Chrystian Quintero Mateus, MS,[*] Maryam Mashayekhi, PhD,[*] Robert W. Mutter, MD,[*,†] Valentin Djonov, MD,[‡] Jennifer M. Fazzari, PhD,[*] Huaping Xiao, MD,[*] Kelsey M. Frechette, MD,[*] Adam J. Wentworth, MS,[§] Jonathan M. Morris, MD,[§] Brandon Klebel,[‖] Jack C. Thull,[*] Rachael M. Guenzel, APRN, CNP, DNP,[*] David J. Schembri Wismayer, MD,[¶] Fabrice Lucien, PhD,[#,**] Sean S. Park, MD, PhD,[*] and Scott C. Lester, MD[*]

[*]*Department of Radiation Oncology, Mayo Clinic, Rochester, Minnesota;* [†]*Department of Molecular Pharmacology and Experimental Therapeutics, Mayo Clinic, Rochester, Minnesota;* [‡]*Institute of Anatomy, University of Bern, Bern, Switzerland;* [§]*Department of Radiology, Mayo Clinic, Rochester, Minnesota;* [‖]*Division of Engineering, Mayo Clinic, Rochester, Minnesota;* [¶]*Division of Anatomic Pathology, Mayo Clinic, Rochester, Minnesota;* [#]*Department of Urology, Mayo Clinic, Rochester, Minnesota; and* [**]*Division of Immunology, Mayo Clinic, Rochester, Minnesota*

Received May 3, 2024; Accepted for publication Jun 29, 2024

Purpose: Minibeam radiation therapy (MBRT) is characterized by the delivery of submillimeter-wide regions of high "peak" and low "valley" doses throughout a tumor. Preclinical studies have long shown the promise of this technique, and we report here the first clinical implementation of MBRT.

Methods and Materials: A clinical orthovoltage unit was commissioned for MBRT patient treatments using 3-, 4-, 5-, 8-, and 10-cm diameter cones. The 180 kVp output was spatially separated into minibeams using a tungsten collimator with 0.5 mm wide slits spaced 1.1 mm on center. Percentage depth dose (PDD) measurements were obtained using film dosimetry and plastic water for both peak and valley doses. PDDs were measured on the central axis for offsets of 0, 0.5, and 1 cm. The peak-to-valley ratio was calculated at each depth for all cones and offsets. To mitigate the effects of patient motion on delivered dose, patient-specific 3-dimensional-printed collimator holders were created. These conformed to the unique anatomy of each patient and affixed the tungsten collimator directly to the body. Two patients were treated with MBRT; both received 2 fractions.

Results: Peak PDDs decreased gradually with depth. Valley PDDs initially increased slightly with depth, then decreased gradually beyond 2 cm. The peak-to-valley ratios were highest at the surface for smaller cone sizes and offsets. In vivo film dosimetry confirmed a distinct delineation of peak and valley doses in both patients treated with MBRT with no dose blurring. Both patients experienced prompt improvement in symptoms and tumor response.

Conclusions: We report commissioning results, treatment processes, and the first 2 patients treated with MBRT using a clinical orthovoltage unit. While demonstrating the feasibility of this approach is a crucial first step toward wider translation, clinical trials are needed to further establish safety and efficacy.

Corresponding author: Michael P. Grams, PhD; E-mail: grams.michael@mayo.edu

Disclosures: No authors have any conflicts of interest to disclose.

Acknowledgments—We thank Dr. Doug Moseley for assistance with the design of the collimator and Dr. Kimberly Corbin for thoughtful review of the manuscript.

Supplementary material associated with this article can be found, in the online version, at doi:10.1016/j.ijrobp.2024.06.035.

Int J Radiation Oncol Biol Phys, Vol. 120, No. 5, pp. 1423–1434, 2024
0360-3016/$ - see front matter
https://doi.org/10.1016/j.ijrobp.2024.06.035

Introduction

Spatially fractionated radiation therapy (SFRT) is a unique form of treatment that intentionally delivers a nonuniform dose consisting of alternating regions of high "peak" and low "valley" doses.[1-3] The technique was originally developed in the early 1900s to reduce skin toxicity when treating deep tumors with the low energy (keV) x-ray sources available at the time.[4] By blocking portions of the radiation with a steel wire net, the skin receiving the lower valley doses of radiation would heal and regenerate, greatly reducing treatment toxicity. In modern clinical practice, much higher (MeV) energy radiation sources are used to treat patients with SFRT using a variety of methods, including photon collimating blocks,[5,6] lattice techniques,[7-9] and proton pencil beam scanning.[10] Because scatter from peak regions into the adjacent valleys is more prevalent at higher energies, the size and spacing of irradiated regions must be on the order of centimeters to maintain the desired nonuniform dose distribution when using these methods. However, by using keV energy x-rays and collimators with narrow slits the width of the irradiated regions can be reduced to 25 to 100 μm with a center-to-center spacing of 50 to 500 μm while still maintaining a high differential between peak and valley doses. Decades of preclinical research have demonstrated that these so-called "microbeams" induce unique biological effects. By reducing the width of the irradiated regions, numerous animal studies have demonstrated extraordinary normal tissue tolerance to peak doses of hundreds or even thousands of Gy.[11-15] Additional preclinical studies have shown microbeams provide excellent tumor control[16-19] and may enhance antitumor immune responses.[20,21]

Despite the abundance of convincing preclinical work, microbeam SFRT has not yet been translated to patients. Due to the extremely narrow and closely spaced microbeams, even the slightest physiologic motion during irradiation could result in blurring of the differential arrangement of peak and valley doses, thereby reducing or eliminating normal tissue sparing.[22] To avoid such blurring, microbeam doses must be delivered with ultrahigh kGy/s dose rates. These dose rates can only be achieved with synchrotron x-ray sources, but only a few synchrotrons in the world can generate microbeams. Furthermore, these facilities are large national laboratories rather than radiation oncology clinics, which, in combination with the technical requirements for microbeams, presents additional obstacles for patient treatments.

To overcome the translational challenges associated with microbeams, "minibeam" radiation therapy (MBRT) was proposed.[23,24] The difference in spatial dimensions is somewhat arbitrary between micro- and minibeams, but minibeams are wider (typically $\geq$ 500 μm) and have a larger center-to-center spacing than microbeams (typically $\geq$ 1000 μm). Although these slightly larger dimensions reduce the peak doses that can be safely delivered,[25] numerous preclinical studies have shown minibeams still offer many of the same benefits as microbeams, including excellent normal tissue sparing, tumor control, and immunomodulation.[23,26-29] Most importantly, because of their larger size and spacing, minibeams are less vulnerable to blurring with physiologic motion. This allows for the use of conventional x-ray sources with lower dose rates, which require more time to deliver a therapeutic dose at depth while still maintaining healthy tissue sparing. Here we report on the commissioning of a clinically available orthovoltage unit for MBRT and the first clinical implementation of this novel approach.

Methods and Materials

Orthovoltage commissioning

The 180 kVp output from an Xstrahl 300 orthovoltage unit (Xstrahl Inc) was used for all measurements and patient treatments. X-ray tube specifications are a half-value layer of 0.5 mm Cu, a focal spot size of 8 mm, and a target angle of 30°. The unit was calibrated for absolute dosimetry according to the American Association of Physicists in Medicine Task Group 61[30] in-air protocol using an ionization chamber calibrated by an accredited dosimetry laboratory. The nominal dose rate for standard, non-MBRT treatments is approximately 200 cGy/min at 1 cm depth in water with a tube current of 10 mA.

Circular cones having a focus-to-source distance of 30 cm and diameters of 3, 4, 5, 8, and 10 cm were commissioned for MBRT. The homogeneous x-ray output from the circular cones was spatially separated into minibeams using custom-made tungsten collimators (Midwest Tungsten Services). Two square collimators were fabricated, one with outer dimensions of 7 $\times$ 7 cm^2 for use with the 3, 4, and 5 cm cones, and the other with outer dimensions of 12 $\times$ 12 cm^2 for use with the 8 and 10 cm cones. The tungsten collimators are 2.5 mm thick and have 0.5 mm wide slits that are spaced 1.1 mm on center (Fig. 1). These dimensions were chosen to be similar to previous in silico and preclinical studies.[24,29,31] Slit lengths are 5 cm and 10 cm for the 7 $\times$ 7 cm^2 and 12 $\times$ 12 cm^2 collimators, respectively. The collimator slits are nondivergent to avoid the complexity that would arise from having to align the collimator with the divergent x-ray beam for patient treatments. Because the tungsten collimator is only 2.5 mm thick, the effects of divergence are small and were deemed clinically acceptable.

Minibeam dosimetry was performed using Gafchromic EBT4 film (Ashland) calibrated with the 180 kVp output from the Xstrahl 300 unit. Film analysis was performed using FilmQA Pro software (Ashland) following the American Association of Physicists in Medicine Task Group 235[32] recommendations and a previously published protocol.[33] Minibeam peak and valley doses were measured in a stack of 30 $\times$ 30 $\times$ 20 cm^3 Plastic Water DT (CIRS), which is suitable for energies as low as 50 keV. A subset of film

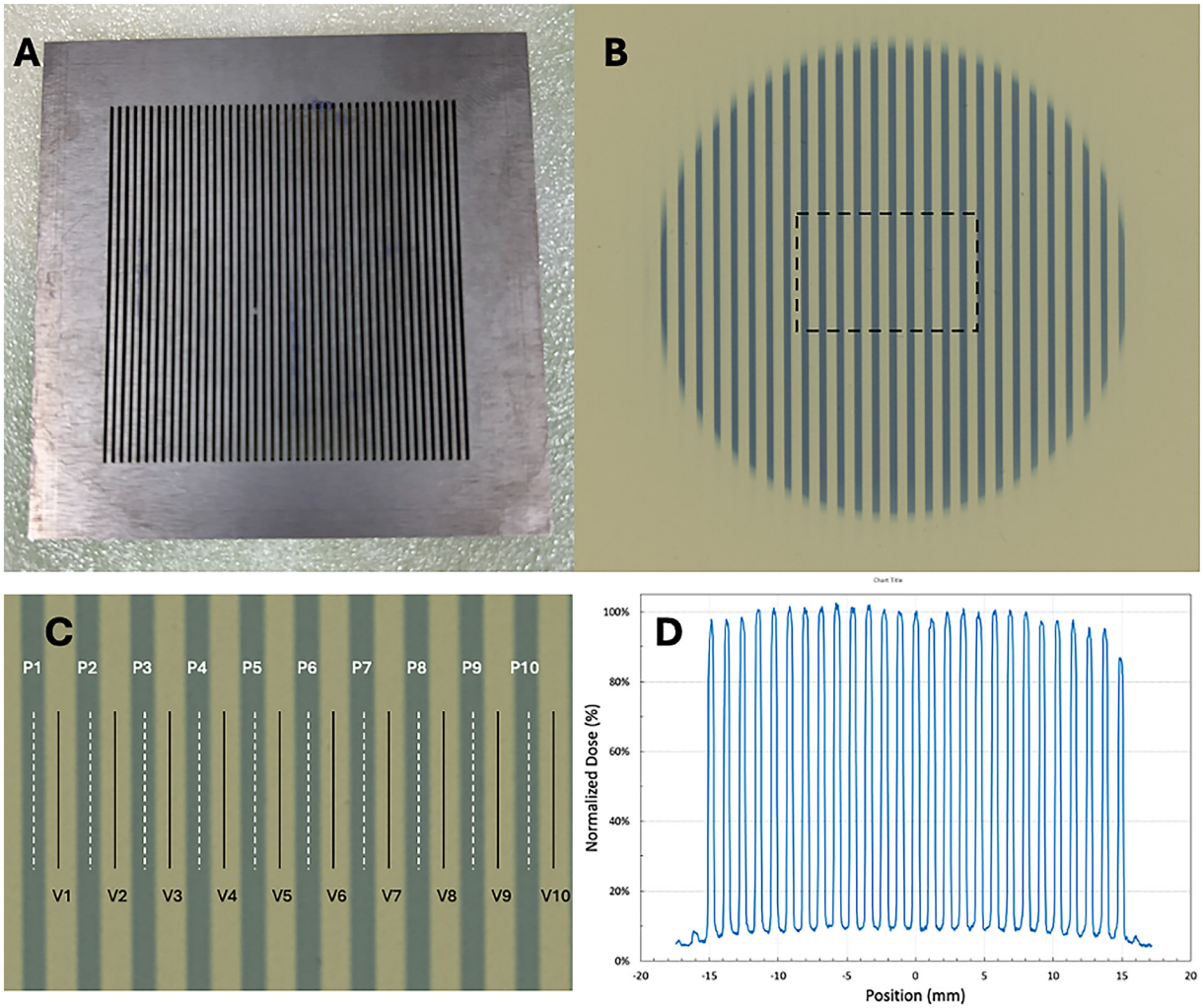

Fig. 1. (A) Photo of the 7 × 7 cm^2 tungsten collimator. (B) Image of film placed on the surface of plastic water and exposed using the 3 cm cone. The rectangular dashed line indicates the central region where the 10 peaks and valleys are sampled for percentage depth dose measurements. (C) Magnified view of the rectangular region shown in (B). The white dashed lines correspond to the 10 peak measurements (P1-P10) and the black solid lines to the 10 valley measurements (V1-V10). Peak widths are 0.5 mm at the surface, and valleys are 0.6 mm wide. The peak and valley doses were averaged over a profile 1 cm long and 200 μm wide. (D) Measured minibeam dose profile of the 3 cm cone exposure shown in (B). The dose is normalized to the central peak.

measurements made in a water tank confirmed agreement between the Plastic Water and liquid water to within 2%. For each circular cone, film measurements were made perpendicular to the axis of the beam from the surface to a depth of 7 cm in 1 cm increments. Measurements were made with the tungsten collimator directly on the plastic water (no offset), as well as with the tungsten collimator offset by 0.5 and 1 cm above the plastic water (Fig. E1). The cone was then placed flush on the surface of the tungsten collimator prior to delivering radiation. The offset measurements were made to better approximate clinical scenarios where, due to anatomical considerations, the tungsten collimator cannot be placed directly on the target. Films were irradiated with 900 monitor units (MUs), which resulted in a peak dose range of approximately 700 cGy at the surface to 100 cGy at 7 cm depth. All measurements were repeated 3 times by 3 separate physicists over the course of 3 months.

More than 24 hours after exposure, an Epson 12000 flatbed scanner was used to scan all films at a resolution of 1200 dpi. Peak and valley doses were obtained at each depth by averaging along a 1 cm long, 200-μm wide line profile positioned on each of the 10 central peaks and adjacent 10 valley regions on each film (Fig. 1C). Because measurements were repeated 3 times, this resulted in a total of 30 central peak and valley dose measurements at each depth. A single representative peak and valley dose for each depth was then calculated from the average of these 30 measurements. By dividing the measured doses by the number of MU delivered, dose rates in cGy/MU were obtained at each depth. These dose rates were then converted to percentage depth dose (PDD) curves to be

used for subsequent dose calculations. PDDs were normalized to the peak dose at 1 cm, which was the chosen prescription depth for patient treatments.

Three-dimensional printed collimator holder

Despite the larger size of minibeams compared to microbeams, patient motion during lengthy treatment times is still a concern due to the low dose rate of the orthovoltage unit. To mitigate the effects of motion, 3-dimensional (3D)-printed collimator holders, which conform to the unique anatomy of each individual patient, were made. The tungsten collimators slide into these holders, which are then affixed directly to the patient. This ensures that if motion occurs, the patient and collimator move together, preserving the integrity of the spatially separated peak and valley doses.

To create the patient-specific collimator holder, a computed tomography (CT) scan of the patient is required. The patient is positioned comfortably with support devices and vacuum cushions as appropriate. If possible, the patient is positioned so the weight of the tungsten collimator helps hold the collimator holder in place rather than pulling it tangentially to either side. For example, a patient with a target on the left neck may be placed in the right lateral decubitus position rather than supine. A 3D rendering of the body surface is obtained from the CT scan, and the physician contours the target. Using the Varian contouring workspace (Varian Medical Systems), a square structure having dimensions of either 7×7 cm^2 or 12×12 cm^2 corresponding to the size of the tungsten collimator appropriate for the target is created. This structure is positioned over the target and oriented as close as possible to the surface while making sure the tungsten collimator will not impinge upon the patient. Once an appropriate orientation is found, the DICOM radiation therapy (RT) structure set is saved and exported into Materialise Mimics Medical software (version 26.0, Materialise N.V.) for the creation of the 3D-printed collimator holder.

The objects contained within the Mimics file include the patient body, target, and collimator structures, which are subsequently moved to Materialise 3-Matic Medical software (version 17.0, Materialise N.V.). An in-house Python script aligns a generic collimator holder template with the tungsten collimator structure in the orientation where the tungsten slides into the holder. Once the tungsten collimator structure and collimator holder are properly located, the generic collimator template is Boolean subtracted from the body surface contour to create the patient-specific collimator holder, which conforms to the patient. The collimator holder is evaluated for any areas that may prevent proper positioning, as well as ensuring adequate points of contact for a conformal fit and stability in the desired location. Any sharp, skin-contacting edges are removed, and the collimator holder is labeled with a unique identifier, fiducials to check dimensional accuracy, and the anatomic location and orientation. Digital mockups of the design are reviewed and approved by a physicist and physician, then exported as stereolithography files for 3D printing with vat photopolymerization technology on a Form 3B printer in Biomed Amber resin (Formlabs). After printing, the part is postprocessed according to manufacturer instructions, and holes are tapped and fitted with 4-48 spring plungers (McMaster Carr) to help secure the tungsten collimator within the collimator holder. Generating a 3D-printed collimator holder can be completed in 24 hours, the majority of which is used for printing and postprocessing. The general process for creating the collimator holder is illustrated in Figure 2.

MBRT treatment process

For treatment, the patient is placed in the same position as the simulation CT scan. The 3D-printed holder is placed on the patient without the tungsten collimator in place, so the physician can clinically confirm the location of the target. Once it is determined that the collimator holder fits appropriately and is comfortable, it is further secured using an elastic strap that attaches to the collimator holder. A small piece of Gafchromic film is placed directly on the target for in vivo dosimetry, and the tungsten collimator is then inserted into the collimator holder. Based on the target size, an appropriate cone diameter is chosen by the physician, and the orthovoltage unit is positioned with the end of the cone in direct contact and flush with the surface of the tungsten collimator. Using the commissioning measurements, MUs are calculated to deliver the prescribed peak dose at 1 cm depth, and treatment is delivered.

The patient is monitored with audio and video during the entire treatment. Due to the small size and spacing of the irradiated regions, along with the inherent uncertainty in day-to-day patient positioning, the peak and valley regions cannot be aligned exactly for multiple treatments. Therefore, for a 2-fraction regimen, the process is repeated on the second day with the collimator rotated by 90° within the collimator holder. This "crossfire" arrangement is commonly used in preclinical studies using fractionation and results in only small overlapping peak regions where the cumulative dose doubles without compromising normal tissue tolerance.[34,35]

Informed consent was obtained from both patients treated with MBRT. The consenting physician thoroughly discussed the novelty of MBRT, the absence of human-specific evidence for safety and efficacy, the proposed rationale for use in their circumstances, and alternative RT and non-RT options. Both patients gave their consent to proceed with MBRT treatment.

Patient 1

A 69-year-old male with newly diagnosed Merkel cell carcinoma involving the left arm, bulky regional adenopathy, and a single metastasis in the pancreas was initiated on pembrolizumab monotherapy.[36] At diagnosis, the mass

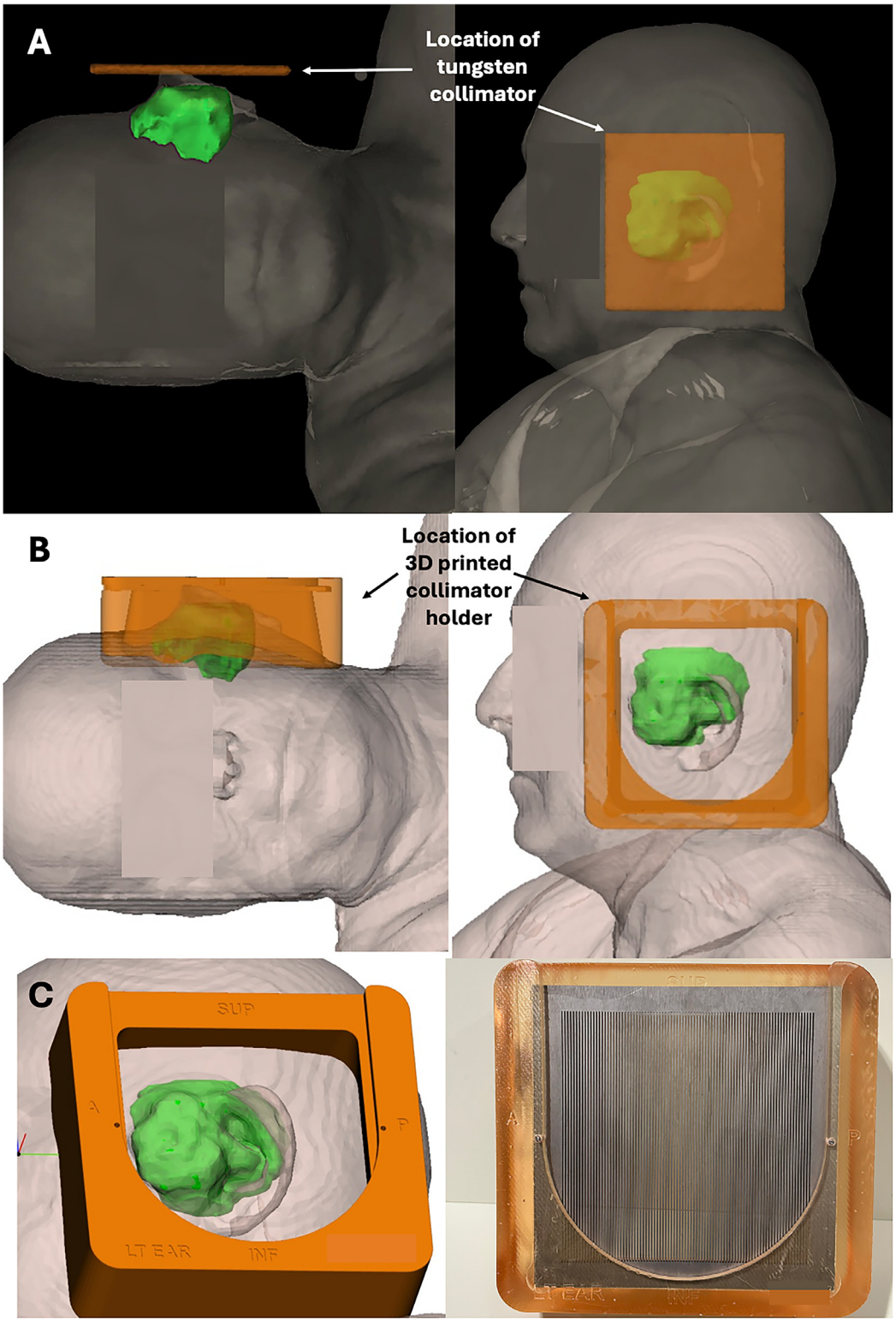

Fig. 2. Process for creating the patient-specific 3-dimensional (3D) collimator holder. (A) A surface rendering of a patient (in lateral decubitus position) along with the target (in green) is created from a computed tomography scan. A square structure representing the 12 × 12 cm^2 tungsten collimator is shown in the appropriate position for treatment. (B) A digital rendering of the 3D-printed collimator holder on the patient. The portion that contacts the patient is Boolean subtracted from the body surface to conform exactly to the patient's anatomy. (C) Closeup view of the 3D-printed collimator holder showing labels that indicate orientation and anatomic location. The photo shows the actual collimator holder with the 12 × 12 cm^2 tungsten collimator in place.

measured 14 × 14 × 11 cm^3 and encased the brachial plexus and subclavian vessels. He reported severe pain in the axilla, discomfort from an inability to adduct his arm below 80°, and radicular-type pain and numbness in his forearm. Given the expected response rate of 56%, an anticipated time to symptom relief of weeks to months, and the intolerable nature of his present symptoms, he was referred to the Department of Radiation Oncology. A multidisciplinary decision was made to utilize MBRT to accelerate tumor regression and shorten the time to symptom relief, while minimizing radiation exposure to preserve normal tissue tolerance for future treatment. Given that he had a single distant metastasis and was motivated for maximal therapy, we planned for the possibility that his future regional treatment would include comprehensive RT to the axilla and supraclavicular fossa. As such, prompt symptom relief was needed from radiation, but it was of paramount importance to minimize exposure to normal tissue. Additionally, because his pain worsened in a supine position, he did not feel he could lay flat for the duration of a conventional RT treatment. He was most comfortable sitting up and could only be treated in this position with the orthovoltage unit. MBRT was delivered between his second and third infusions of pembrolizumab. The patient was prescribed a peak dose of 1500 cGy per fraction at 1 cm depth to be delivered daily for a total of 2 fractions using a 10-cm diameter cone. The radiation delivery time was approximately 11.5 minutes for each fraction. Despite using the largest available cone size, the entire target could not be covered so the treatment field was directed toward the centermost region of the tumor.

Patient 2

A 74-year-old male with a history of chronic lymphocytic leukemia was referred to the Department of Radiation Oncology for a multiply recurrent preauricular squamous cell carcinoma. This had been last treated 6 months prior with a local excision. He had avoided seeking subspecialty care because of mistrust in the healthcare system and fear of general anesthesia. The lesion now measured 7 × 6 × 3 cm^3 in size and completely occluded the external auditory canal, causing ipsilateral conductive hearing loss, shooting pain, and intermittent bleeding. He was initiated on cemiplimab. Shortly after his first infusion, the lesion swelled. This was accompanied by severe unrelenting pain that was unresponsive to acetaminophen and ibuprofen. Additionally, the lesion began to continuously secrete frank blood. Despite the patient's hesitancy with anesthesia, his ultimate goal was to maximize his chances of survival. To meet this goal, we felt he would be best served with a surgical resection and tissue reconstruction. However, at the time of consultation, he was unable to consider moving forward with surgery because of his prior experience with anesthesia and severe pain. After thoroughly counseling him, we provided hydromorphone for analgesia and administered 2 fractions of MBRT. The goal of MBRT was to urgently mitigate pain and bleeding without antagonizing his immunotherapy or complicating future local therapies by reducing the chances of normal tissue toxicity. The patient was prescribed a peak dose of 1500 cGy per fraction at 1 cm depth to be delivered daily for a total of 2 fractions using a 5-cm diameter cone. The radiation delivery time was approximately 12 minutes for each fraction.

Results

PDDs and peak-to-valley ratios

PDD curves for both peak and valley doses as well as the peak-to-valley ratio (PVR) as a function of depth for no offset are plotted in Figure 3. The corresponding data for the 0.5 and 1 cm offsets is qualitatively similar and is included in the supplementary materials (Figs. E2-12). The peak PDDs decrease gradually with depth due to attenuation, reaching 50% between 3.5 and 4 cm. Because the PDDs are normalized to 1 cm, peak surface doses range from 125% to 130%, depending on cone size and offset. Slightly larger peak PDD values were seen with larger cone sizes. MBRT peak dose rates at 1 cm depth ranged from 110 to 120 cGy/min, with higher peak dose rates corresponding to larger cone sizes and smaller offsets. The 3 independent PDD measurements for each cone, depth, and offset provided consistent results with a median standard deviation of 0.8% (range, 0.3%-3.6%).

The main contributor to the valley dose is scatter from adjacent peak regions.[37] Near the surface, scatter from peak regions initially increases with depth before eventually decreasing due to attenuation of the peak dose. Accordingly, valley PDDs were lowest at the surface and increased with depth before reaching a plateau from 1 to 2 cm. Beyond 2 cm, valley PDDs decrease slowly with depth due to the decreasing peak doses. Valley PDDs were larger for larger cone sizes and offsets.

PVRs were highest at the surface for smaller cone sizes and smaller offsets, ranging from a PVR of 11 for the 3 cm cone with no offset to a PVR of 6 for the 10 cm cone and 1 cm offset. Due to increasing scatter into the valley regions, PVRs decreased rapidly within 1 cm, after which they decreased more gradually.

In vivo dosimetry

In vivo films placed directly on both patients over the target areas for all fractions confirmed a distinct delineation of peak and valley dose regions with no evidence of blurring despite the low dose rate of the orthovoltage system. The first fraction films and resulting dose distributions for both patients are shown in Figure 4. Surface dose measurements for the second fraction were similar to the first for each respective patient (not shown). Since the tungsten collimator was rotated 90° between the first and second fractions, the cumulative

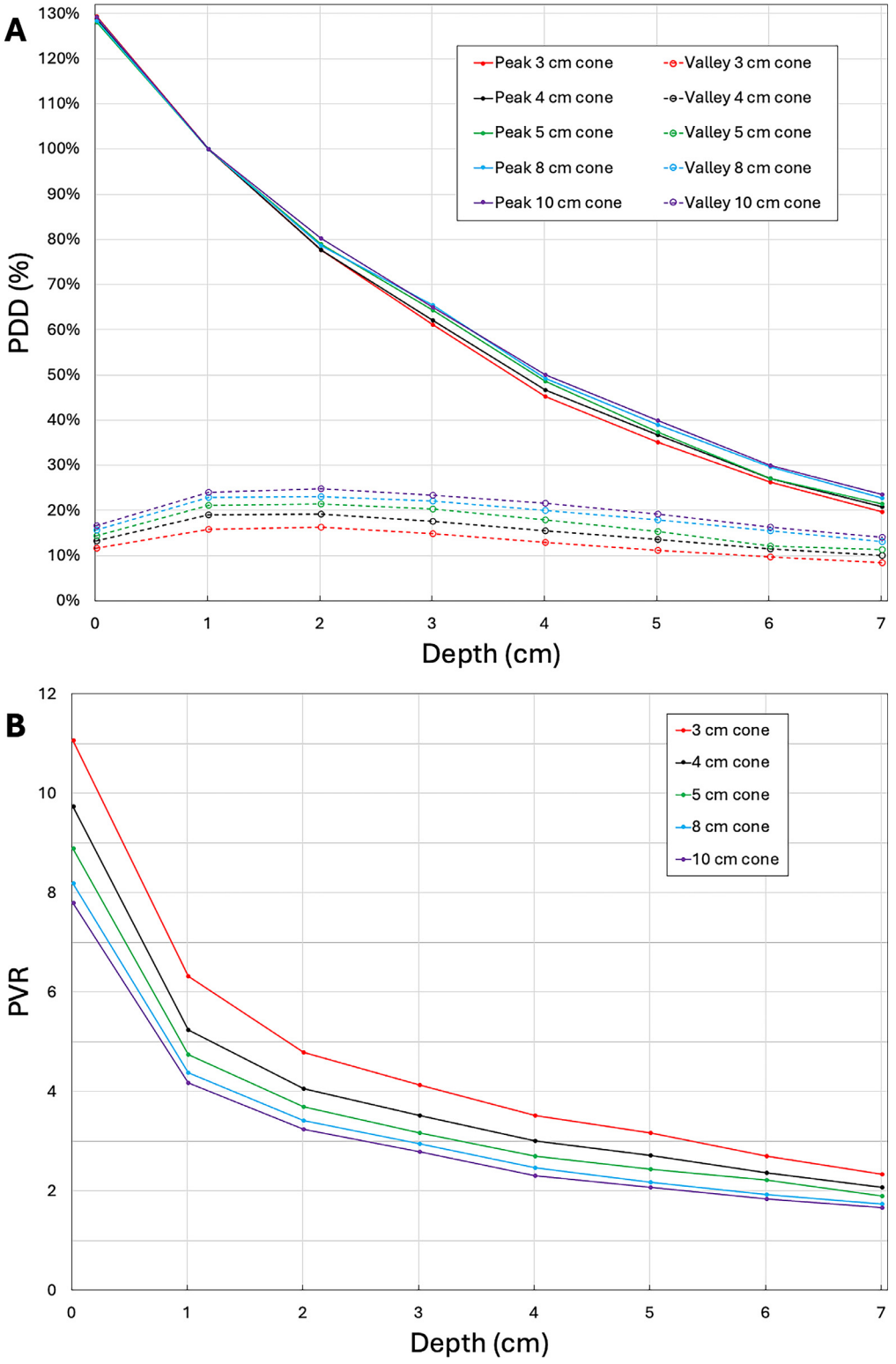

Fig. 3. Peak and valley percentage depth doses (PDDs) and peak-to-valley ratios (PVRs) as a function of depth for zero offset. (A) PDDs are normalized to the peak dose at 1 cm depth. Both peak and valley PDDs are shown. Peak PDDs are generally similar, with larger cone sizes having larger PDDs at depth. The valley PDDs are greater for the larger cone sizes and initially increase before leveling off and decreasing gradually. (B) Measured PVRs for each cone decrease rapidly over the first 1 cm before decreasing more gradually with depth. PVR is inversely related to cone size.

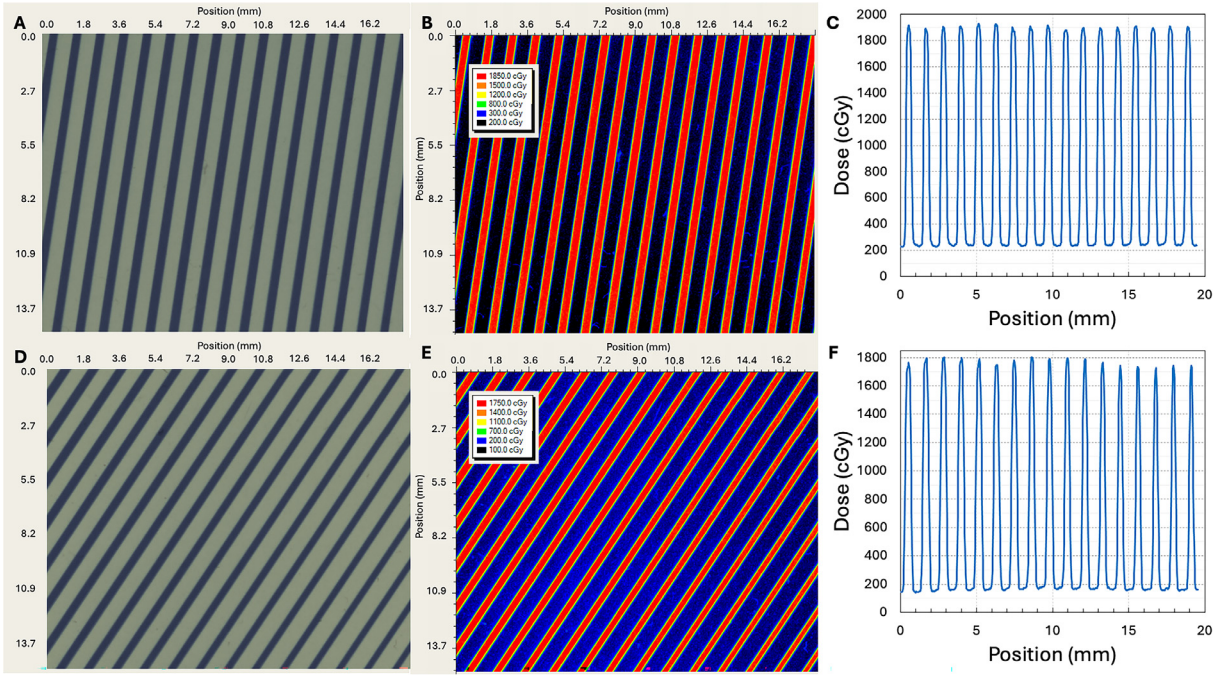

Fig. 4. In vivo film dosimetry for patients 1 and 2 confirmed no evidence of dose blurring despite low dose rates. Films were placed on the surface of the target and show a distinct delineation of peak and valley doses delivered with minibeam radiation therapy. Note the difference in dose scales. (A) Gafchromic EBT4 in vivo film for patient 1, (B) two-dimensional (2D) colorwash depiction of the delivered dose, and (C) corresponding dose profile. (D) Gafchromic EBT4 in vivo film for patient 2; (E) 2D colorwash depiction of the delivered dose; and (F) corresponding dose profile.

maximum peak and valley doses delivered at the surface in overlapping regions of the "crossfire" arrangement were twice the measured values for each individual patient.

Based on the PDD measurement for the 10-cm cone obtained during commissioning, the expected single fraction peak and valley doses at the surface for patient 1 (axillary tumor) were 2017 cGy and 258 cGy, respectively. Gafchromic EBT4 film placed directly on the surface of the tumor during treatment measured peak and valley doses of 1900 and 230 cGy, respectively. Based on the PDD measurement for the 5-cm cone obtained during commissioning, the expected single fraction peak and valley doses at the surface for patient 2 (ear tumor) were 1938 cGy and 248 cGy, respectively. The measured peak and valley doses obtained from EBT4 film placed on the surface of the target were 1800 and 180 cGy, respectively.

Patient 1 treatment response

Figure 5A-D shows a digital rendering of the patient's surface for creation of the collimator holder and treatment photos. After one fraction, his caregiver noted an immediate decrease in the degree of exudate during dressing changes. Six days after the second fraction of MBRT, the patient reported resolution of axillary pain, improvement in range of motion, and near-complete cessation of bleeding and discharge. He was seen again in clinic 3 weeks after MBRT. The mass continued to shrink rapidly, his full range of motion was restored, and an updated CT showed the treated mass was $6.5 \times 12.3 \times 10$ cm^3. He was undergoing a modest response in the nontreated lesions and was experiencing progressive plexopathic symptoms in the forearm, likely due to brachial plexus compression from unirradiated supraclavicular disease. Tumor response 23 days after MBRT is displayed in Figure 5E-F. He had persistent disease in the axilla and supraclavicular fossa. Approximately 2 months after receiving MBRT, he received 4005 cGy in 15 fractions of conventional external beam RT at his local hospital. He experienced a small area of moist desquamation in the axilla where skin was absent due to the initial bulky tumor that had erupted through the epidermis. He was evaluated 4 weeks after his conventional treatment and demonstrated a clinical complete response to all sites of disease.

Patient 2 treatment response

A photo of the tumor on the day of MBRT and the treatment setup are shown in Figure 6A-B. After one fraction, the degree of exudate improved markedly. Six days later, his pain and bleeding completely abated, and he reported subjective improvement in his hearing. Thirty-four days after MBRT, he continued to be asymptomatic, and the lesion had completely flattened. Figure 6C-D shows tumor response after 16 and 34 days, respectively. He experienced

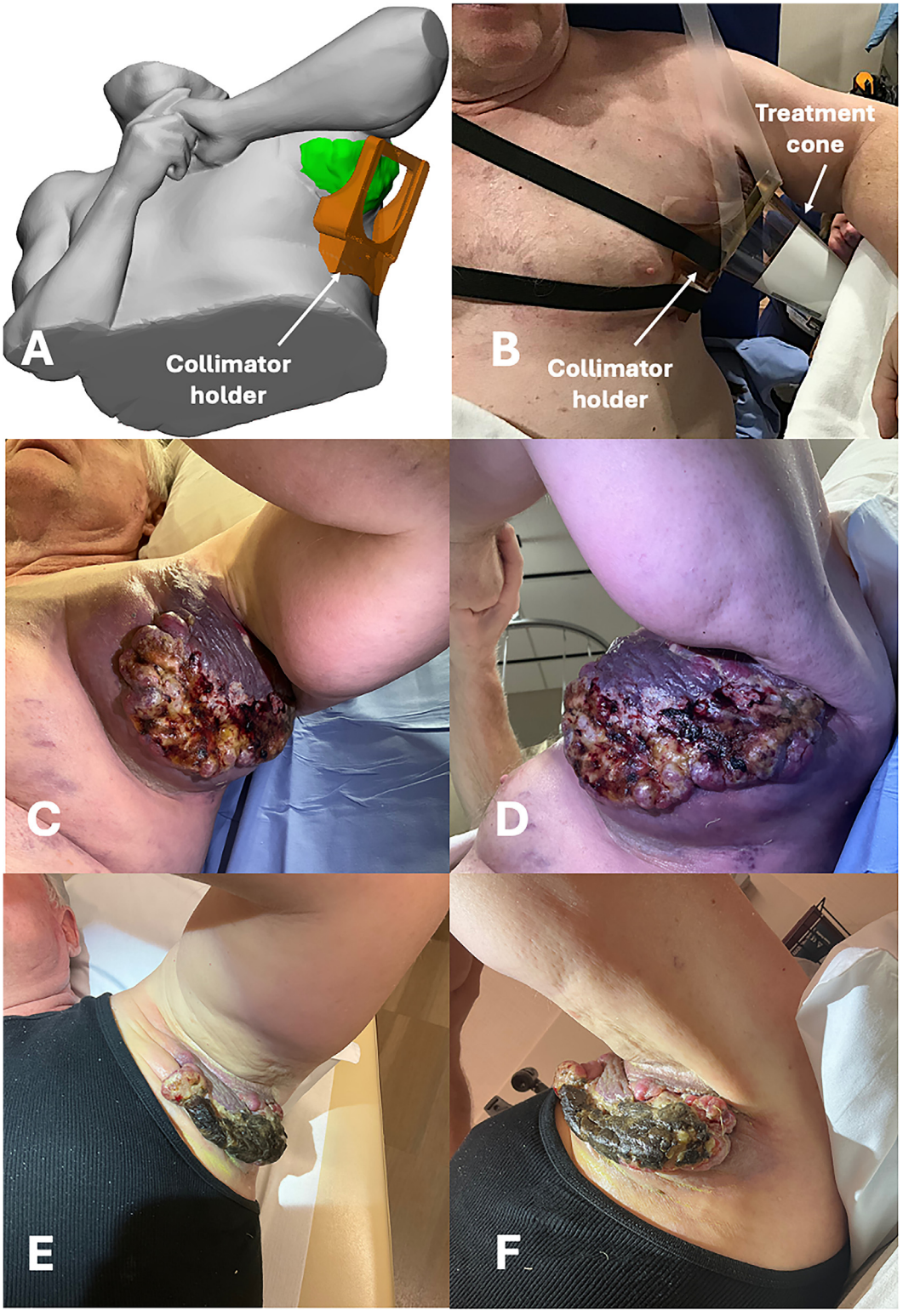

Fig. 5. Treatment photos and response for patient 1. (A) Three-dimensional (3D) rendering of the patient's surface, tumor (in green), and collimator holder (in orange). Due to pain, the patient could not adduct the arm below 80°. (B) Treatment photo showing the location of collimator holder in the same position as shown in (A) and the treatment cone. (C) Anterior and (D) lateral photos of the tumor on the day of treatment. (E) Anterior and (F) lateral photos of tumor response 23 days after treatment.

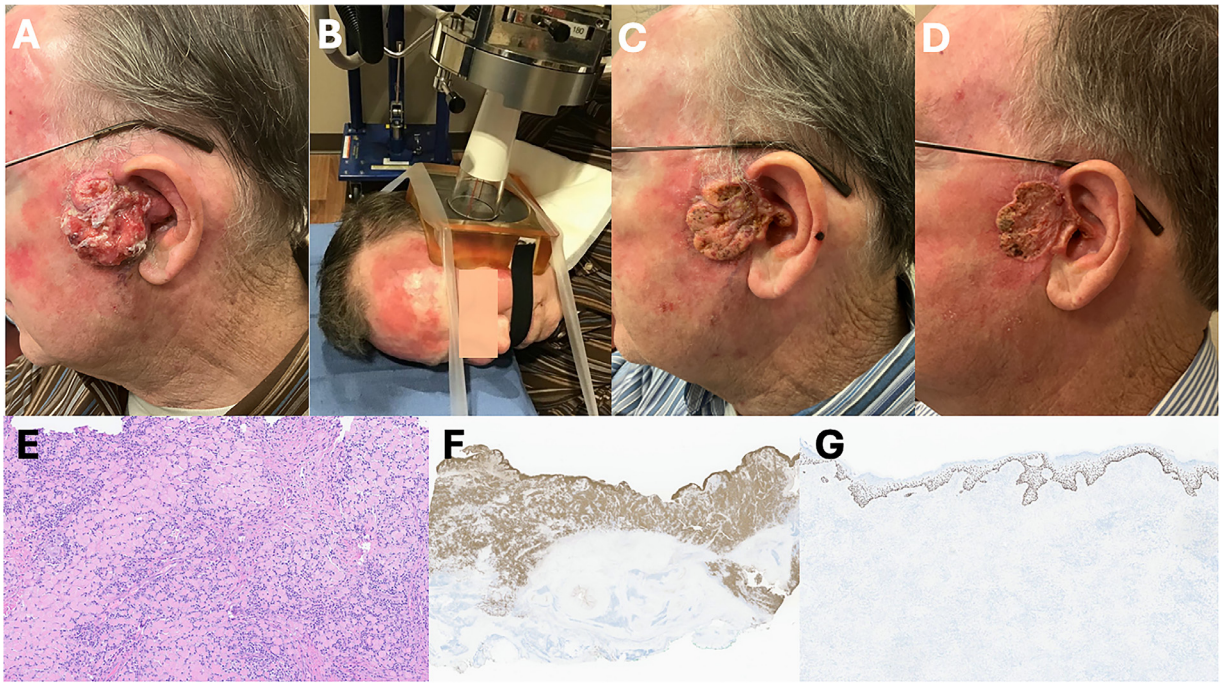

Fig. 6. Treatment photos, response, and pathology for patient 2. (A) Photo of the tumor on the day of minibeam radiation therapy (MBRT). (B) Treatment photo showing the patient in lateral decubitus position with the collimator holder attached, the 5 cm cone flush and in contact with the tungsten collimator. (C) Tumor response 16 days and (D) 34 days after MBRT. (E) Hematoxylin and eosin stain of tumor sample showing extensive necrotic keratinocytes that are without nuclei mixed with a lymphocytic infiltrate. These extend from the surface (top of the image) deep into the tissue. (F) Keratin stain demonstrating keratinocytes, confirming the extent of the tumor bed deep to the patient surface. (G) The corresponding p40 immunohistochemical stain shows the absence of nuclei in the keratinocytes except in the regenerating basal skin layer. Higher resolution pathology images are included in the supplementary materials.

no discernible acute effects from MBRT. Additionally, the patient was very pleased with the outcome, trusted our team, and was now willing to reconsider our recommendation for a standard of care resection. He underwent a total parotidectomy, temporal bone resection, neck dissection, and radial forearm free flap reconstruction. Final pathology demonstrated a tumor bed of necrotic keratinocytes extending into the dermis with an extensive histiocytic reaction (Fig. 6E-G, Figs. E13-15). There were scant areas of epithelial islands with mild atypia deeper into the tissue concerning for residual viable foci of squamous or possibly regenerating epithelium. This was distinct from the marked atypia in the initial biopsy specimen. Given the excellent response, adjuvant radiation was not recommended.

Discussion

In this paper, we report our commissioning results, treatment processes, and the first 2 patients ever treated with MBRT using a clinical orthovoltage unit. The motivation for our work came from decades of thoughtful and convincing preclinical experiments which showed treatment with submillimeter wide beams of radiation can produce remarkable biological benefits. The majority of these previous studies were performed with synchrotron x-ray sources capable of ultrahigh kGy/s dose rates; however, the fact that these sources are not widely accessible hindered clinical translation. Here we have demonstrated a clinically feasible method for treating patients with MBRT, and we report initial results for 2 patients who experienced prompt pain relief and tumor response after only 2 fractions. Despite treating with dose rates many orders of magnitude lower than synchrotron sources, we have shown with in vivo dosimetry that the integrity and spatial distribution of the minibeam peak and valley regions can be maintained by using a patient-specific collimator holder that conforms and attaches directly to the patient. Both patients experienced effective palliation with evidence of treatment response.

We envision several potential clinical applications for this novel treatment approach that warrant further investigation. Relative to conventional uniform radiation, preclinical studies[23,27,29,31,38] have shown the therapeutic index is increased with MBRT, which facilitates dose escalation and increased normal tissue tolerance. Investigations of MBRT for common clinical scenarios may be especially appealing, namely radioresistant tumors with low probability of tumor control using standard techniques and treatment of previously irradiated areas where normal tissue tolerance is reduced. Additionally, MBRT might also be useful as a boost

in combination with conventional radiation treatment.[39,40] Finally, MBRT may enhance other therapies as preclinical studies have shown MBRT can enhance drug delivery[41] and the effectiveness of immunotherapy.[21,28,42] In both patients reported here, immunotherapy was administered prior to MBRT, but typical responses associated with immunotherapy were felt to be inadequate for symptom improvement. The potential for increasing the efficacy of systemic treatment with MBRT is particularly intriguing, and it is noteworthy that both patients reported here received immunotherapy prior to MBRT with minimal effect, yet evidence of tumor response and symptomatic improvement were realized immediately after administration of MBRT. However, it should be emphasized that associating this rapid response with MBRT is speculative without a larger cohort and in the setting of a clinical trial.

The cone size used to treat both patients did not fully encompass the cross-sectional extent of the tumors; however, a uniform decrease in volume was still observed. This effect was most pronounced for patient 1, where a 10 cm diameter cone was employed to treat a target with an initial cross-sectional size of 14 cm × 14 cm. Additionally, the dose in the peak regions decreased to approximately 50% of prescription at 4 cm depth within the target, yet a substantial 63% reduction in volume occurred within just 3 weeks. While the patient responses reported here highlight the potential of MBRT, it is essential to acknowledge that an understanding of the underlying biological mechanisms remains incomplete. Clinical trials utilizing a standardized treatment approach are necessary to assess acute and late outcomes, and further research examining potential biomarkers (particularly with regard to immune modulation) is needed to advance our understanding of MBRT treatments. Despite establishing the feasibility of our approach, we acknowledge several limitations and opportunities for improvement. The low energy x-rays that are required for MBRT limit the utility of this approach to relatively shallow targets. The choice to use the 180 kVp orthovoltage output for this initial work rather than a higher energy was driven by a compromise between delivering adequate dose to superficial tumors while limiting the dose to underlying critical structures. However, higher energy minibeams have several beneficial characteristics,[37] which could make them attractive for some clinical scenarios and will be characterized in future work.

While we have shown it is possible to deliver MBRT to patients with a clinical orthovoltage unit, the relatively low dose rate of this machine remains another area for improvement. A higher dose rate would more easily allow for dose escalation and deliver treatments more rapidly, further mitigating the risk of motion during treatment. Although it remains to be seen if peak doses in the 100s of Gy are feasible and beneficial for tumor control in humans, investigations of the delivery of these high doses would be more practical with higher dose rate x-ray sources. Furthermore, higher dose rates would allow for clinical investigations of the efficacy of smaller (25-100 μm in width) microbeams. Conventional x-ray sources are not practical in this sense, as the reduced output from the narrow slits in the microbeam collimators would make treatment times prohibitively long. Several potential sources have been proposed and are under active development.[43,44]

Another opportunity for improvement lies in the accurate calculation of MBRT dose distributions. Our in vivo dosimetry results underscore this need, as differences between calculated and delivered doses were evident. Due to the consistency of our commissioning measurements, we attribute these discrepancies to dissimilarities between the flat, homogeneous geometry used for those measurements and the nonuniform surfaces and heterogeneity associated with patients. Patient 1 had a large tumor that was somewhat flat and homogeneous, and the agreement between in vivo measurement and expected peak and valley doses at the surface was within approximately 10%. However, patient 2 had a round, apical tumor overlying both bone and air cavities, and an approximately 28% difference was seen between the calculated and measured valley dose. The shape and heterogeneity associated with this target strongly affect the scatter characteristics of the kV x-rays, and the lower valley dose measurement can be understood since scatter is a primary contributor to the valley dose. MBRT dose calculations are not trivial due to the submillimeter scale and low beam energies, yet accurate dosimetry will be critical for correlating delivered doses with therapeutic outcomes. Monte Carlo methods have been extensively used to model synchrotron microbeams[45-47] and could be extended to conventional x-ray sources for clinical MBRT treatments. The 3-D Monte Carlo dose calculations would also allow for quantification of the cumulative dosimetry related to the crossfire MBRT beam arrangement. Treatment responses may differ with this arrangement compared to those that attempt to align the peak and valley regions, and knowledge of dosimetric parameters such as mean dose, equivalent uniform dose, and other SFRT-relevant dosimetric parameters will be crucial to assess the efficacy of MBRT.

Finally, although our work provides a crucial first step toward a wider translation of this novel approach, a formal phase 1 trial is needed to further establish safety. We are designing a phase 1 dose escalation trial to determine the recommended phase 2 dose of MBRT. The results of that study are expected to inform subsequent trials aimed at examining the efficacy of MBRT alone or as part of combination therapy.

References

1. Griffin RJ, Ahmed MM, Amendola B, et al. Understanding high-dose, ultra-high dose rate, and spatially fractionated radiation therapy. *Int J Radiat Oncol Biol Phys* 2020;107:766-778.
2. Billena C, Khan AJ. A current review of spatial fractionation: back to the future? *Int J Radiat Oncol Biol Phys* 2019;104:177-187.
3. Prezado Y. Divide and conquer: spatially fractionated radiation therapy. *Expert Rev Mol Med* 2022;24:e3.
4. Marks H. A new approach to the roentgen therapy of cancer with the use of a grid. *J Mt Sinai Hosp N Y* 1950;17:46-48.
5. Zhang H, Wu X, Zhang X, et al. Photon GRID radiation therapy: A physics and dosimetry white paper from the Radiosurgery Society (RSS) GRID/LATTICE, Microbeam and FLASH Radiotherapy Working Group. *Radiat Res* 2020;194:665-677.

6. Mohiuddin M, Stevens JH, Reiff JE, Huq MS, Suntharalingam N. Spatially fractionated (GRID) radiation for palliative treatment of advanced cancer. *Radiat Onco Investig* 1996;4:41-47.
7. Grams MP, Owen D, Park SS, et al. VMAT grid therapy: a widely applicable planning approach. *Pract Radiat Oncol* 2021;11:e339-e347.
8. Duriseti S, Kavanaugh J, Goddu S, et al. Spatially fractionated stereotactic body radiation therapy (Lattice) for large tumors. *Adv Radiat Oncol* 2021;6: 100639.
9. Wu X, Ahmed MM, Wright J, Gupta S, Pollack A. On modern technical approaches of three-dimensional high-dose lattice radiotherapy (LRT). *Cureus* 2010;2:e9.
10. Gao M, Mohiuddin MM, Hartsell WF, Pankuch M. Spatially fractionated (GRID) radiation therapy using proton pencil beam scanning (PBS): feasibility study and clinical implementation. *Med Phys* 2018;45:1645-1653.
11. Slatkin DN, Spanne P, Dilmanian FA, Gebbers JO, Laissue JA. Subacute neuropathological effects of microplanar beams of x-rays from a synchrotron wiggler. *Proc Natl Acad Sci U S A* 1995;92:8783-8787.
12. Laissue J, Blattmann H, Di Michiel M, et al. Weanling piglet cerebellum: a surrogate for tolerance to MRT (microbeam radiation therapy) in pediatric neuro-oncology. *Paper presented at: International Symposium on Optical Science and Technology*. San Diego, CA.
13. Laissue JA, Barre S, Bartzsch S, et al. Tolerance of normal rabbit facial bones and teeth to synchrotron x-ray microbeam irradiation. *Radiat Res* 2022;197:233-241.
14. Serduc R, van de Looij Y, Francony G, et al. Characterization and quantification of cerebral edema induced by synchrotron x-ray microbeam radiation therapy. *Phys Med Biol* 2008;53:1153-1166.
15. Brönnimann D, Bouchet A, Schneider C, et al. Synchrotron microbeam irradiation induces neutrophil infiltration, thrombocyte attachment and selective vascular damage in vivo. *Sci Rep* 2016;6:33601.
16. Bouchet A, Lemasson B, Le Duc G, et al. Preferential effect of synchrotron microbeam radiation therapy on intracerebral 9L gliosarcoma vascular networks. *Int J Radiat Oncol Biol Phys* 2010;78:1503-1512.
17. Dilmanian FA, Button TM, Le Duc G, et al. Response of rat intracranial 9L gliosarcoma to microbeam radiation therapy. *Neuro Oncol* 2002;4:26-38.
18. Griffin RJ, Koonce NA, Dings RP, et al. Microbeam radiation therapy alters vascular architecture and tumor oxygenation and is enhanced by a galectin-1 targeted anti-angiogenic peptide. *Radiat Res* 2012;177:804-812.
19. Potez M, Fernandez-Palomo C, Bouchet A, et al. Synchrotron microbeam radiation therapy as a new approach for the treatment of radioresistant melanoma: potential underlying mechanisms. *Int J Radiat Oncol Biol Phys* 2019;105:1126-1136.
20. Trappetti V, Potez M, Fernandez-Palomo C, et al. Microbeam radiation therapy controls local growth of radioresistant melanoma and treats out-of-field locoregional metastasis. *Int J Radiat Oncol Biol Phys* 2022;114:478-493.
21. Bazyar S, O'Brien III ET, Benefield T, et al. Immune-mediated effects of microplanar radiotherapy with a small animal irradiator. *Cancers (Basel)* 2021;14:155.
22. Duncan M, Donzelli M, Pellicioli P, et al. First experimental measurement of the effect of cardio-synchronous brain motion on the dose distribution during microbeam radiation therapy. *Med Phys* 2020;47:213-222.
23. Dilmanian FA, Zhong Z, Bacarian T, et al. Interlaced x-ray microplanar beams: a radiosurgery approach with clinical potential. *Proc Natl Acad Sci U S A* 2006;103:9709-9714.
24. Prezado Y, Martinez-Rovira I, Thengumpallil S, Deman P. Dosimetry protocol for the preclinical trials in white-beam minibeam radiation therapy. *Med Phys* 2011;38:5012-5020.
25. Sammer M, Teiluf K, Girst S, et al. Beam size limit for pencil minibeam radiotherapy determined from side effects in an in-vivo mouse ear model. *PLoS One* 2019;14: e0221454.
26. Rivera JN, Kierski TM, Kasoji SK, Abrantes AS, Dayton PA, Chang SX. Conventional dose rate spatially-fractionated radiation therapy (SFRT) treatment response and its association with dosimetric parameters-A preclinical study in a Fischer 344 rat model. *PLOS ONE* 2020;15: e0229053.
27. Bazyar S, Inscoe CR, O'Brian ET, Zhou O, Lee YZ. Minibeam radiotherapy with small animal irradiators; in vitro and in vivo feasibility studies. *Phys Med Biol* 2017;62:8924-8942.
28. Bertho A, Iturri L, Brisebard E, et al. Evaluation of the role of the immune system response after minibeam radiation therapy. *Int J Radiat Oncol Biol Phys* 2023;115:426-439.
29. Deman P, Vautrin M, Edouard M, et al. Monochromatic minibeams radiotherapy: from healthy tissue-sparing effect studies toward first experimental glioma bearing rats therapy. *Int J Radiat Oncol Biol Phys* 2012;82:e693-e700.
30. Ma CM, Coffey CW, DeWerd LA, et al. AAPM protocol for 40-300 kV x-ray beam dosimetry in radiotherapy and radiobiology. *Med Phys* 2001;28:868-893.
31. Prezado Y, Deman P, Varlet P, et al. Tolerance to dose escalation in minibeam radiation therapy applied to normal rat brain: long-term clinical, radiological and histopathological analysis. *Radiat Res* 2015;184:314-321.
32. Niroomand-Rad A, Chiu-Tsao ST, Grams MP, et al. Report of AAPM Task Group 235 radiochromic film dosimetry: an update to TG-55. *Med Phys* 2020;47:5986-6025.
33. Howard ME, Herman MG, Grams MP. Methodology for radiochromic film analysis using FilmQA Pro and ImageJ. *PLOS ONE* 2020;15: e0233562.
34. Serduc R, Bräuer-Krisch E, Bouchet A, et al. First trial of spatial and temporal fractionations of the delivered dose using synchrotron microbeam radiation therapy. *J Synchrotron Radiat* 2009;16:587-590.
35. Fernandez-Palomo C, Trappetti V, Potez M, et al. Complete remission of mouse melanoma after temporally fractionated microbeam radiotherapy. *Cancers (Basel)* 2020;12:2656.
36. Nghiem PT, Bhatia S, Lipson EJ, et al. PD-1 blockade with pembrolizumab in advanced merkel-cell carcinoma. *N Engl J Med* 2016;374:2542-2552.
37. Prezado Y, Thengumpallil S, Renier M, Bravin A. X-ray energy optimization in minibeam radiation therapy. *Med Phys* 2009;36:4897-4902.
38. Prezado Y, Dos Santos M, Gonzalez W, et al. Transfer of minibeam radiation therapy into a cost-effective equipment for radiobiological studies: a proof of concept. *Sci Rep* 2017;7:17295.
39. Potez M, Bouchet A, Flaender M, et al. Synchrotron x-ray boost delivered by microbeam radiation therapy after conventional x-ray therapy fractionated in time improves F98 glioma control. *Int J Radiat Oncol Biol Phys* 2020;107:360-369.
40. Serduc R, Bouchet A. MRT-boost as the last fraction may be the most efficient irradiation schedule for increased survival times in a rat glioma model. *J Synchrotron Radiat* 2023;30:591-595.
41. Sabatasso S, Fernandez-Palomo C, Hlushchuk R, et al. Transient and efficient vascular permeability window for adjuvant drug delivery triggered by microbeam radiation. *Cancers (Basel)* 2021;13:2103.
42. Johnsrud AJ, Jenkins SV, Jamshidi-Parsian A, et al. Evidence for early stage anti-tumor immunity elicited by spatially fractionated radiotherapy-immunotherapy combinations. *Radiat Res* 2020;194:688-697.
43. Yuan H, Zhang L, Frank JE, et al. Treating brain tumor with microbeam radiation generated by a compact carbon-nanotube-based irradiator: initial radiation efficacy study. *Radiat Res* 2015;184:322-333.
44. Winter J, Galek M, Matejcek C, et al. Clinical microbeam radiation therapy with a compact source: specifications of the line-focus X-ray tube. *Phys Imaging Radiat Oncol* 2020;14:74-81.
45. Paino J, Cameron M, Large M, et al. DoseMRT: a software package for individualised Monte Carlo dose calculations of synchrotron-generated microbeam radiation therapy. *Radiation* 2023;3:123-137.
46. Day LRJ, Donzelli M, Pellicioli P, et al. A commercial treatment planning system with a hybrid dose calculation algorithm for synchrotron radiotherapy trials. *Phys Med Biol* 2021;66: 055016.
47. Kraus KM, Winter J, Zhang Y, et al. Treatment planning study for microbeam radiotherapy using clinical patient data. *Cancers (Basel)* 2022;14:685.